Nanoparticle Acoustic Resonance Enhanced Nearly-Degenerate Four-Wave Mixing

Dao Xiang and Reuven Gordon*

Department of Electrical and Computer Engineering, University of Victoria, Victoria, BC, V8W3P6, Canada.

ABSTRACT: Nanoparticles have acoustic resonances in the 10 GHz to THz range, which makes them interesting for resonantly enhanced four-wave mixing applications such as frequency conversion. Using a nearly-degenerate four-wave mixing setup and comparing with Rayleigh-Gans-Debye scattering, we estimate a nonlinear refractive index, n_2, of approximately 2×10^{-5} cm^2/MW for 22 nm polystyrene nanospheres in water at a difference frequency of 43 GHz. This is nearly three orders of magnitude larger than the typical below-bandgap nonlinear response of semiconductors. This strong high-frequency response may be ideal for four-wave frequency conversion in all-optical information technologies, with appropriately chosen nanoparticle sizes.
KEYWORDS: *nonlinear nanophotonics, nanoparticles, acoustic vibration, four-wave mixing.*

The nonlinear optical response of materials is typically weak, since photons do not interact strongly with matter. For four-wave mixing (FWM) applications, the nonlinear refractive index, n_2, is ~2×10^{-8} cm^2/MW at high frequency (in the hundreds of THz)[1]. This requires high powers for applications such as FWM wavelength conversion. Much stronger nonlinear responses can be found for phase transitions[2], low-dimensional materials[3-11], and gradient forces on nanoparticles[12,13], with responses of ~3.6×10^{-3} cm^2/MW. These are all very slow processes, due to the slow response of phase transitions or transport of nanoparticles over macroscopic distances. As a result, they are not suitable applications like high frequency shift wavelength conversion. Faster approaches, up to ~10 GHz, include stimulated Brillouin scattering[14,15] and nonlinear mixing in semiconductor amplifiers and waveguides[16-24]. For even higher frequency conversion in the >20 GHz to several THz range (which is the target of all-optical data processing, since it is faster than what is easily achievable with electronics alone), processes that involve electrostriction can be considered.

Stimulated Raman scattering typically makes use of molecular vibrations, but it is relatively weak. It has been recognized, however, that large-scale vibrations of nanoparticles can give strong Raman response[25-29]. Nanoparticles have also been investigated by the pump-probe spectroscopy, particularly for metal nanoparticles[30-32]. For wavelength conversion applications, metal nanoparticles may not be the best candidates because they have substantial absorption at their plasmonic resonance[33].

Recently, we reported on acoustic vibrations of individual nanoparticles and proteins in an optical tweezer setup[34]. Intrigued by the large response of these individual dielectric nanoparticles, here we measure the nearly-degenerate FWM (NDFWM) of polystyrene nanoparticles in aqueous solution. The acoustic resonance frequencies measured by NDFWM match well with our previous experiments and also agree with Lamb's theory, and the nonlinear response is almost three orders of magnitude higher than the intrinsic response of semiconductors. This opens up exciting possibility for nanoscale size-tunable efficient wavelength conversion.

Figure 1 shows the NDFWM configuration used to study the acoustic resonance enhanced nonlinear scattering of dielecric nanoparticles. A continuous-wave (CW) tunable distributed Bragg reflector laser (DBR852P, Thorlabs) and a CW tunable external-cavity laser (DL 100, Toptica Photonics) supply counter-propagating optical beams with wavelength around 853 nm to illuminate the sample region and the external-cavity laser has the shorter wavelength. After passing two lenses with focal lengths of 5 cm and 4 cm, the collimated distributed Bragg reflector laser beam diameter is 43.5 μm and the collimated external-cavity laser beam size is 18 μm × 54 μm. The nonlinear medium was an aqueous suspension of polystyrene nanoparticles with 1% weight/volume concentration (3000 series, Thermo Scientific, with typical diameter dispersion below 1 nm) in a quartz cuvette where the anti-reflection coating on cell windows helps reduce surface reflection losses.

The polarization controller and polarizer ensured co-polarized illumination. The angle between the pump beam with amplitude A_1 and the probe beam with amplitude A_3 was adjusted to ~6º to allow for three hundred micrometer nonlinear interaction length $L=a\times(1/\tan\theta+1/\sin\theta)$, where a is the width of laser beam, θ is the angle between two laser beams. The optical chopper modulated the intensity of the pump wave A_2 to only permit the Rayleigh scattered light of the pump wave A_2 and the Bragg-diffracted beam with amplitude A_4 to be measured by an avalanche photodetector (APD120A, Thorlabs) and amplified by a lock-in amplifier (SR510, Stanford Research Systems). The power of the distributed Bragg reflector laser was fixed to a relatively small value of 10 mW to limit the amplitude of Rayleigh scattered light (which will be used for power estimation in the next part), while the power of external-cavity laser was set to a relatively high value of 60 mW to excite two beams of the four-wave mixing process.

The frequency difference between the two laser sources was scanned with a step of 1 GHz, and the nonlinear response was recorded at the avalanche photodetector. A variable optical attenuator was used to obtain the power dependence of the nonlinear response at acoustic resonance.

The inelastic scattering can be understood from Figure 1. The interference between the pump beam A_2 at frequency ω_2 and the probe beam A_3 at frequency ω_3 induces a travelling

periodic variation in refractive index of the sample via the electrostrictive force that elongates individual nanoparticles along the polarization direction. Another pump wave A_1 at frequency ω_1 ($\omega_1 = \omega_3 > \omega_2$) Bragg diffracts off the electrostriction induced moving grating and is red-shifted due to the Doppler effect. This creates a signal wave A_4 with frequency $\omega_4 = \omega_1 + \omega_2 - \omega_3 = \omega_2$.

When the beat frequency $\Omega=\omega_3-\omega_2$ is tuned to the acoustic resonance, the acoustic vibration modes of the polystyrene nanoparticles will be resonantly excited. The resulting resonant oscillation of the spheroid eccentricity creates a strong refractive index perturbation, that is, the moving grating.

Now we consider the phase matching condition in this scheme and assume that the propagation directions of the pump wave and the probe wave are along $\mathbf{z}'$ and $\mathbf{z}$ axes, respectively, and the in-plane direction perpendicular to $\mathbf{z}'$ is along the $\mathbf{y}'$ axis. The wavevector mismatching term becomes

$$\begin{aligned}\overrightarrow{\Delta k} &= \overrightarrow{k_1} + \overrightarrow{k_2} - \overrightarrow{k_3} - \overrightarrow{k_4} \\ &= n_s \frac{\omega_2 - \omega_1}{c}\hat{z}' - n_s \frac{\omega_4 - \omega_3}{c}\hat{z} \\ &= n_s \frac{\Omega}{c}(1-\cos\theta)\hat{z} - n_s \frac{\Omega}{c}\sin\theta\hat{y} \end{aligned} \quad (1)$$

where n_s is the refractive index of solvent; c is the light velocity in vacuum; $\hat{y}, \hat{z}, \hat{z}'$ are unit vectors. Because the angle between two laser beams θ is 6° and the interaction length is three hundred micrometers, the phase mismatch $\Delta\boldsymbol{k}\cdot\boldsymbol{L}$ is small and can be ignored.

Figure 2 shows the avalanche photodiode detected signal at the chopped frequency as the function of the beat frequency between distributed Bragg reflector laser and external cavity laser for polystyrene nanoparticles with a diameter of 22 nm. The error bars are from repeated measurements. It is also noticed that the non-resonant background would drop by 0.1 mV after blocking the external-cavity laser because the gradient force plays a role in moving nanoparticles into the high-field regions[12].

It is noted that there is an acoustic resonance peak with full width at half maximum (FWHM) of ~2 GHz located at 43 GHz. This value matches well with the theoretical prediction of the quadrupolar accordion mode (l=2, n=0) based on Lamb's theory[35]. In the theoretical calculations, the transverse sound velocity and longitudinal sound velocity of polystyrene were taken to be 2350 m/s and 1120 m/s[36].

It is interesting to note that the linewidth is quite narrow; however, this is not unprecedented for nanoparticles in solution. For example, the damping time for acoustic vibrations in a sample of bipyramidal gold nanoparticles, capped with polystyrene sulphonic acid, in water was measured to be 261±10 ps[37], indicating a 4 GHz bandwidth for those larger nanoparticles. Our measurement shows a smaller bandwidth for smaller nanoparticles, while our larger particles give a larger bandwidth because of higher damping (~5 GHz for the 30 nm particles and ~6 GHz for the 40 nm particles, not shown). A smaller resonant response was observed for those larger nanoparticles, and so we focus on the results for the 22 nm nanoparticles for the remainder.

Figure 3 shows the NDFWM peak frequencies for different nanoparticle diameters. The error bars on the sphere diameter is the manufacture's specification. All the above results are consistent with our previous nanotweezers work[34] (including the appearance of a smaller peak seen at close to 70 GHz in Figure 2). We note that in the present configuration the $l = 0$ peak is barely visible. We found that the ratio between the powers is power-dependent and this may be related to the power required for the nonlinear response to exceed the background scattering. We were unable to explore higher powers to test this hypothesis due to limitations in the laser output.

To estimate the strength of nonlinearity at the acoustic resonance, we compared the wavelength conversion from coupled-wave theory in nonlinear optics[38] to the scattering from Rayleigh-Gans-Debye theory[39]. By assuming, for simplicity, that all of waves have the plane wavefronts and the pump depletion effect is neglected, and solving the coupled-wave equations, the intensity of signal wave at the incident plane of the probe wave z=0 is given by

$$I_4(0) = \tan^2\left(|\kappa|L\right) I_3(0) \approx |\kappa|^2 L^2 I_3(0) \quad (2)$$

where $|\kappa| = \frac{3\omega}{n_s c}\chi^{(3)}|A_1||A_2| = \frac{3\pi}{\varepsilon_0 n_s^2 c\lambda}\chi^{(3)}\sqrt{I_1 I_2}$; n_s is the refractive index of solvent; c is the light velocity in vacuum; $\chi^{(3)}$ is the effective third-order susceptibility of medium; ε_0 is the vacuum permittivity; λ is the wavelength of light; and L is the light-matter interaction length. The approximation in Eq. (2) is reasonable considering $|\kappa|L \approx 0.0003$.

The Rayleigh-Gans-Debye theory can be employed to describe the linear light scattering of colloidal sample. The intensity of scattered light collected at the angle θ at a distance d_0 from the sample is

$$I_{RGD,2} = R_{RGD} I_2 = \frac{f(\theta)}{d_0^2} N\Delta\rho^2 V_p^2 P(q) S(q, c_i) I_2 \quad (3)$$

where $f(\theta)=3\cos^2\theta$ is a geometrical factor accounting for the orientation of the transition dipole moment relative to the incident laser field; $N = c_i \times V$ is the number of nanoparticles in the illuminated volume, where c_i is the number concentration and $V = \pi(a/2)^2 \times b/\sin\theta$ (a is the collimated DBR laser beam diameter and b is the optical aperture size of APD); the scattering length density difference $\Delta\rho$ reflecting for the scattering ability of the sample is expressed as

$$\Delta\rho = \frac{3\pi n_s^2}{\lambda^2}\frac{m^2-1}{m^2+2} \quad (4)$$

with relative refractive index $m = n_p/n_s$ between the nanoparticle (n_p) and the solvent (n_s); V_p is the nanoparticle volume; the modulus of scattering vector is given by

$$q = \frac{4\pi}{\lambda} n_s \sin(\frac{\theta}{2}); \quad (5)$$

the form factor describing the intra-nanoparticle interference for a nanoparticle with radius of r_p is given by[40]

$$P(q) = \frac{9}{(qr_p)^6}\left[\sin(qr_p) - qr_p\cos(qr_p)\right]^2; \quad (6)$$

the structure factor $S(q, c_i)$ describing the inter-nanoparticle interference is the function of q and number concentration c_i, and it is expressed as[41]

$$S(q) \approx 1 - \frac{1}{3}\left(qR_g\right)^2 \quad (7)$$

with the radius of gyration R_g.

After combining Eqs. (2) and (3), the estimation of $\chi^{(3)}$ is given by

$$\chi^{(3)} = \sqrt{\frac{I_4 \cdot R_{RGD}}{\left(\frac{3\pi}{\varepsilon_0 n_s^2 c\lambda}\right)^2 L^2 I_1 I_{RGD,2} I_3}} \quad (8)$$

We find that for the 22 nm nanospheres, the third-order susceptibility $\chi^{(3)}$ is 1.8×10^{-17} m^2/V^2 and the nonlinear refractive index n_2 is 2×10^{-5} cm^2/MW. This estimate is three orders of magnitude larger than the intrinsic below bandgap response of silicon[1].

We can also provide a direct calculation of the nonlinear scattering based on the measured response of the APD where the signal height of ~0.5 mV corresponds to the real generated power of ~4.5 nW for the signal wave. We can obtain that the third-order susceptibility $\chi^{(3)}$ is 3.8×10^{-17} m^2/V^2 and the nonlinear refractive index n_2 is 4.3×10^{-5} cm^2/MW by Eq. (2). These values are close to those calculated with Rayleigh-Gans-Debye theory, supporting the reliability of the estimation.

Figure 4 shows the external-cavity laser power dependence of the nonlinear signal strength (i.e., subtracting the non-resonant background from Rayleigh scattering) by manually adjusting a variable optical attenuator. An approximately quadratic power dependence is seen as expected since we are varying the intensity of two beams in the NDFWM. It is noted that the starting point is 40 mW, which we believe is due to the large Rayleigh background that swamps out the signal below this value.

Actually, this narrow bandwidth in Figure 2 is not ideal for ultra-fast switching of the wavelength conversion. In that case, more disperse nanoparticles may be considered, or a more viscous solution[37]. For wavelength conversion that is modulated at less than a GHz, this narrow bandwidth can be appropriate if we tune the nanoparticle size to match the frequency conversion requirement. In the present work, we have not demonstrated the wavelength conversion due to challenges in the setup, where the nanowatts of nonlinear signal generation is overwhelmed by the nearly-degenerate milliwatts of pump power. Nevertheless, the nonlinear susceptibility is for that process is expected to be almost identical to the one measured here. The size scaling is shown in Figure 3, and scales inversely with radius. Another possibility is to tune the material properties, such as mechanical structure or material type.

In conclusion, we have demonstrated acoustic resonance enhanced NDFWM using the electrostriction-induced vibrations of dielectric nanoparticles in solution. The role of the acoustic resonant vibration was confirmed by the characteristic resonant peak positions as compared with Lamb's theory. Our experiments with an aqueous suspension of 22 nm nanospheres showed a nonlinear refractive index n_2 is 2×10^{-5} cm^2/MW, which is three orders of magnitude larger than the intrinsic response of silicon, but two orders of magnitude weaker than the gradient-force induced Kerr nonlinearity from nanoparticle displacement.

The observed narrow-band response is interesting, although it is not unprecedented for nanoparticles. This is not desirable for fast switching, where the critical damping condition is desired to get the maximum bandwidth response. In subsequent studies, we intend to investigate other nonlinear nanomaterials to achieve such a broadband response, as well as applying this effect in frequency conversion application[42].

AUTHOR INFORMATION

Corresponding Author

* Email: rgordon@uvic.ca.

Funding Sources

This work is supported by the NSERC CREATE grant Materials for Enhanced Energy Technologies.

ACKNOWLEDGMENT

The authors acknowledge financial support from the Natural Sciences and Engineering Research Council CREATE grant.

REFERENCES

(1) Lin, Q.; Zhang, J.; Piredda, G.; Boyd, R. W.; Fauchet, P. M.; Agrawal, G. P. Dispersion of silicon nonlinearities in the near infrared region. *Appl. Phys. Lett.* **2007**, 91, 21111.

(2) Khoo, I. C. Nonlinear optics of liquid crystalline materials. *Phys. Rep.* **2009**, 471, 221-267.

(3) Miller, D. A. B.; Chemla, D. S.; Eilenberger, D. J.; Smith, P. W.; Gossard, A. C.; Wiegmann, W. Degenerate four-wave mixing in room-temperature GaAs/GaAlAs multiple quantum well structures. *Appl. Phys. Lett.* **1983**, 42, 925-927.

(4) Feuerbacher, B. F.; Kuhl, J.; Ploog, K. Biexcitonic contribution to the degenerate-four-wave-mixing signal from a GaAs/Al_xGa_{1-x} As quantum well. *Phys. Res. B* **1991**, 43, 2439.

(5) Yang, L.; Becker, K.; Smith, F. M.; Magruder, R. H.; Haglund, R. F.; Yang, L.; Dorsinville, R.; Alfano, R. R. Zuhr, R.A. Size dependence of the third-order susceptibility of copper nanoclusters investigated by four-wave mixing. *J. Opt. Soc. Am. B* **1994**, 11, 457-461.

(6) Akiyama, T.; Wada, O.; Kuwatsuka, H.; Simoyama, T.; Nakata, Y.; Mukai, K.; Sugawara, M.; Ishikawa, H. Nonlinear processes responsible for nondegenerate four-wave mixing in quantum-dot optical amplifiers. *Appl. Phys. Lett.* **2000**, 77, 1753-1755.

(7) Renger, J.; Quidant, R.; van Hulst, N.; Palomba, S.; Novotny, L. Free-space excitation of propagating surface plasmon polaritons by nonlinear four-wave mixing. *Phys. Rev. Lett.* **2009**, 103, 266802.

(8) Renger, J.; Quidant, R.; Van Hulst, N.; Novotny, L. Surface-enhanced nonlinear four-wave mixing. *Phys. Rev. Lett.* **2010**, 104, 046803.

(9) Zhang, Y.; Wang, Z.; Nie, Z.; Li, C.; Chen, H.; Lu, K.; Xiao, M. Four-wave mixing dipole soliton in laser-induced atomic gratings. *Phys. Rev. Lett.* **2011**, 106, 093904.

(10) Kauranen, M.; Zayats, A. V. Nonlinear plasmonics. *Nature Photon.* **2012**, 6, 737-748.

(11) Zhang, Y.; Wen, F., Zhen, Y. R.; Nordlander, P.; Halas, N. J. Coherent Fano resonances in a plasmonic nanocluster enhance optical four-wave mixing. *Proc. Natl. Acad. Sci.* **2013**, 110, 9215-9219.

(12) Smith, P. W.; Ashkin, A.; Tomlinson W. J. Four-wave mixing in an artificial Kerr medium. *Opt. lett.* **1981**, 6, 284-286.

(13) Smith, P. W.; Maloney, P. J.; Ashkin, A. Use of a liquid suspension of dielectric spheres as an artificial Kerr medium. *Opt. lett.* **1982**, 7, 347-349.

(14) Ippen, E. P.; Stolen, R. H. Stimulated Brillouin scattering in optical fibers. *Appl. Phys. Lett.* 1972, 21, 539-541.
(15) Zhu, Z.; Gauthier, D. J.; Boyd, R. W. Stored light in an optical fiber via stimulated Brillouin scattering. *Science* **2007**, 318, 1748-1750.
(16) Yoo, S. B. Wavelength conversion technologies for WDM network applications. *J. Lightwave Technol.* **1996**, 14, 955-966.
(17) Girardin, F.; Graziani, L.; Martelli, F.; Spano, P.; Mecozzi, A.; Scotti, S.; Ara, R. D.; Eckner, J.; Guekos, G. Four-wave mixing in semiconductor optical amplifiers: A practical tool for wavelength conversion. *IEEE J. Sel. Topics Quantum Electron.* **1997**. 3, 522-528.
(18) Diez, S.; Schmidt, C.; Ludwig, R.; Weber, H. G.; Obermann, K.; Kindt, S.; Koltchanov, I.; Petermann, K. Four-wave mixing in semiconductor optical amplifiers for frequency conversion and fast optical switching. *IEEE J. Sel. Topics Quantum Electron.* **1997**, 3, 1131-1145.
(19) Geraghty, D. F.; Lee, R. B.; Verdiell, M.; Ziari, M.; Mathur, A.; Vahala, K. J. Wavelength conversion for WDM communication systems using four-wave mixing in semiconductor optical amplifiers. *IEEE J. Sel. Topics Quantum Electron.* **1997**, 3, 1146-1155.
(20) Fukuda, H.; Yamada, K., Shoji, T.; Takahashi, M.; Tsuchizawa, T.; Watanabe, T.; Takahashi, J. I.; Itabashi, S. I. Four-wave mixing in silicon wire waveguides. *Opt. Express* **2005**, 13, 4629-4637.
(21) Dadap, J. I.; Panoiu, N. C.; Chen, X.; Hsieh, I. W.; Liu, X.; Chou, C. Y.; Dulkeith, E.; McNab, S. J.; Xia, F.; Green, W. M. J.; Sekaric, L. Nonlinear-optical phase modification in dispersion-engineered Si photonic wires. *Opt. Express* 2008, 16, 1280-1299.
(22) Salem, R., Foster, M. A.; Turner, A. C.; Geraghty, D. F.; Lipson, M.; Gaeta, A. L. Signal regeneration using low-power four-wave mixing on silicon chip. *Nature Photon.* **2008**, 2, 35-38.
(23) Leuthold, J.; Koos, C.; Freude, W. Nonlinear silicon photonics. *Nature Photon.* **2010**, 4, 535-544.
(24) Liu, X.; Osgood, R. M.; Vlasov, Y. A.; Green, W. M. Mid-infrared optical parametric amplifier using silicon nanophotonic waveguides. *Nature Photon.* **2010**, 4, 557-560.
(25) Fujii, M.; Hayashi, S.; Yamamoto, K. Raman scattering from quantum dots of Ge embedded in SiO_2 thin films. *Appl. Phys. Lett.* **1990**, 57, 2692–2694.
(26) Nie, S.; Emory, S. R. Probing single molecules and single nanoparticles by surface-enhanced Raman scattering. *Science* **1997**, 275, 1102–1106.
(27) Campion, A.; Kambhampati, P. Surface-enhanced Raman scattering. *Chem. Soc. Rev.* 1998, 27, 241–250.
(28) Cao, Y. C.; Jin, R.; Mirkin, C. A. Nanoparticles with Raman spectroscopic fingerprints for DNA and RNA detection. *Science* **2002**, 297, 1536-1540.
(29) Yadav, H. K.; Gupta, V.; Sreenivas, K.; Singh, S. P.; Sundarakannan, B.; Katiyar, R. S. Low frequency Raman scattering from acoustic phonons confined in ZnO nanoparticles. *Phys. Rev. Lett.* **2006**, 97, 085502.
(30) Bigot, J. Y.; Merle, J. Y.; Cregut, O.; Daunois, A. Electron dynamics in copper metallic nanoparticles probed with femtosecond optical pulses. *Phys. Rev. Lett.* **1995**, 75, 4702.
(31) Itoh, T.; Asahi, T.; Masuhara, H. Femtosecond light scattering spectroscopy of single gold nanoparticles. *Appl. Phys. Lett.* **2001**, 79, 1667-1669.
(32) Muskens, O. L.; Del Fatti, N.; Vallée, F. Femtosecond response of a single metal nanoparticle. *Nano Lett.* **2006**, 6, 552-556.
(33) Link, S.; El-Sayed, M.A. Size and temperature dependence of the plasmon absorption of colloidal gold nanoparticles. *J. Phys. Chem. B* 1999, 103, 4212-4217.
(34) Wheaton, S.; Gelfand, R. M.; Gordon, R. Probing the Raman-active acoustic vibrations of nanoparticles with extraordinary spectral resolution. *Nature Photon.* **2015**, 9, 68-72.
(35) Lamb, H. On the vibrations of an elastic sphere. *Proc. London Math. Soc.* **1881**, 1, 189-212.
(36) Lide, D.R. *CRC handbook of chemistry and physics.* CRC Press: Boca Raton, **2004**.
(37) Pelton, M.; Sader, J. E.; Burgin, J.; Liu, M.; Guyot-Sionnest, P.; Gosztola, D. Damping of acoustic vibrations in gold nanoparticles. *Nature Nanotech.* **2009**, 4, 492–495.
(38) Boyd, R. W. *Nonlinear optics 3rd edn*. Academic press: New York, **2008**.
(39) van de Hulst, H. C. *Light Scattering by Small Particles.* John Wiley & Sons: New York, **1957**.
(40) Oster, G.; Riley, D. P. Scattering from isotropic colloidal and macro-molecular systems. *Acta Crystallogr.* **1952**, 5, 1-6.
(41) Mulholland, G.W.; Zhou, L.; Zachariah, M. R.; Heinson, W. R.; Chakrabarti, A.; Sorensen, C. Light scattering shape diagnostics for nano-agglomerates. *Aerosol Sci. & Tech.* **2013**, 47, 520-529.
(42) Cotter, D.; Manning, R.J.; Blow, K.J.; Ellis, A.D.; Kelly, A.E.; Nesset, D.; Phillips, I.D.; Poustie, A.J.; Rogers, D.C. Nonlinear optics for high-speed digital information processing." *Science* **1999**, 286, 1523-1528.

For Table of Contents Use Only

Nanoparticle Acoustic Resonance Enhanced Nearly-Degenerate Four-Wave Mixing
Dao Xiang and Reuven Gordon*

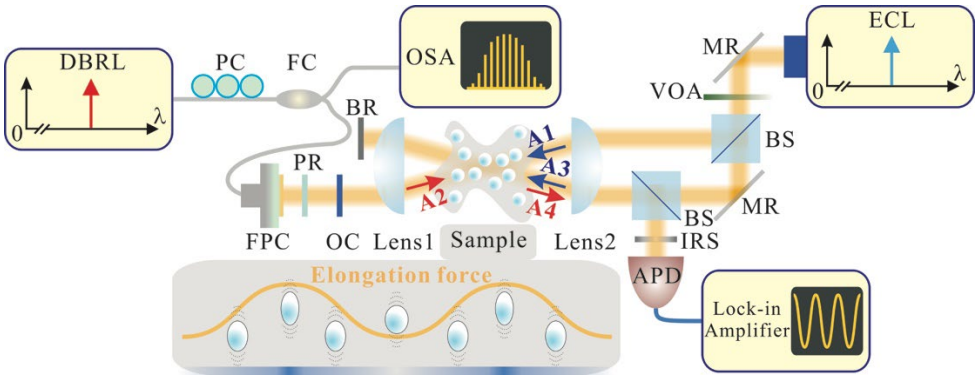

Figure 1. Experimental configuration of NDFWM. DBRL: distributed Bragg reflector laser; PC: polarization controller; FC: fiber coupler; OSA: optical spectrum analyzer; BR: blocker; FPC: fiber-port collimator; PR: polarizer; OC: optical chopper; IRS: iris; APD: avalanche photodetector; BS: beam splitter; MR: mirror; VOA: variable optical attenuator; ECL: external cavity laser.

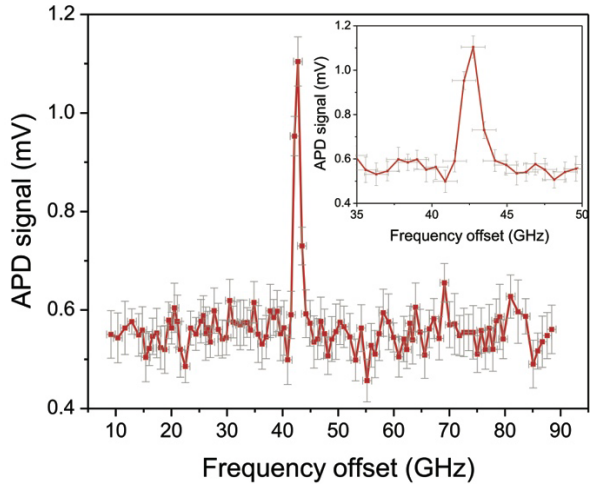

Figure 2. Avalanche photodetector response of an aqueous suspension of 22 nm polystyrene nanoparticles.

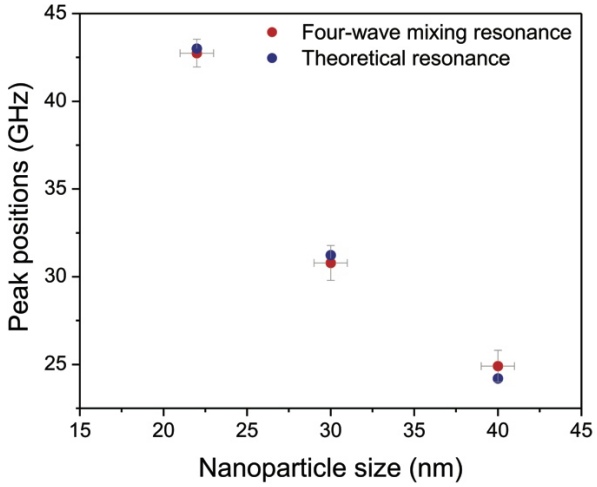

Figure 3. The experimentally confirmation of peak positions against the theoretical values for three different sizes.

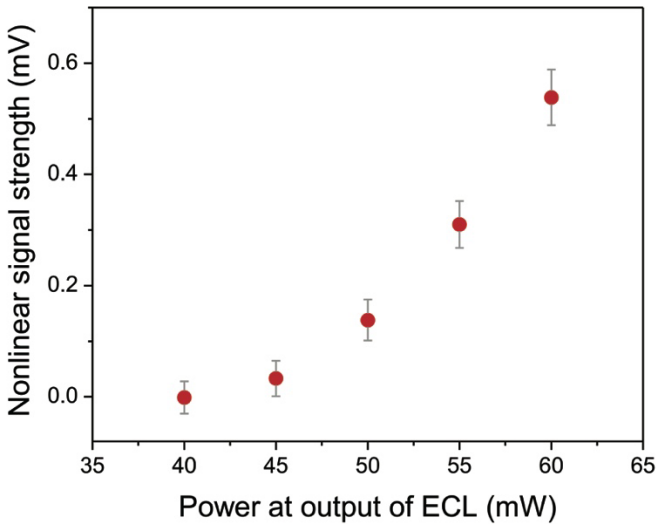

Figure 4. Power dependence of NDFWM at beat frequency 43 GHz for an aqueous suspension of 22 nm polystyrene nanoparticles.